

# Long-term variability of high-mass X-ray binaries. I. Photometry<sup>★</sup>

P. Reig<sup>1,2</sup> and J. Fabregat<sup>3</sup>

<sup>1</sup> IESL, Foundation for Research and Technology-Hellas, 71110, Heraklion, Greece

<sup>2</sup> Physics Department, University of Crete, 71003, Heraklion, Greece e-mail: pau@physics.uoc.gr

<sup>3</sup> Observatorio Astronómico, Universidad de Valencia, E-46100 Burjassot, Spain

Received ; accepted

## ABSTRACT

We present photometric observations of the field around the optical counterparts of high-mass X-ray binaries. Our aim is to study the long-term photometric variability in correlation with their X-ray activity and derive a set of secondary standard stars that can be used for time series analysis. We find that the donors in Be/X-ray binaries exhibit larger amplitude changes in the magnitudes and colours than those hosting a supergiant companion. The amplitude of variability increases with wavelength in Be/X-ray binaries and remains fairly constant in supergiant systems. When time scales of years are considered, a good correlation between the X-ray and optical variability is observed. The X-rays cease when optical brightness decreases. These results reflect the fact that the circumstellar disk in Be/X-ray binaries is the main source of both optical and X-ray variability. We also derive the colour excess,  $E(B - V)$ , selecting data at times when the contribution of the circumstellar disk was supposed to be at minimum, and we revisit the distance estimates.

**Key words.** X-rays: binaries – stars: neutron – stars: binaries close – stars: emission line, Be

## 1. Introduction

Neutron star high-mass X-ray binaries (HMXB) are accretion-powered binary systems where the neutron star orbits an early-type (O or B) companion. The luminosity class of the optical companion subdivides HMXBs into Be/X-ray binaries (BeXB), when the optical star is a dwarf, subgiant, or giant OBe star (luminosity class III, IV, or V), and supergiant X-ray binaries (SXRBS), if they contain an evolved star with luminosity class I-II star. In SXRBS, the optical star emits a substantial stellar wind, removing between  $10^{-6} - 10^{-8} M_{\odot} \text{ yr}^{-1}$  with a terminal velocity up to  $2000 \text{ km s}^{-1}$ . A neutron star in a relatively close orbit will capture a significant fraction of this wind, sufficient to power a bright X-ray source. In BeXB, the donor is a Be star, i.e. a rapidly rotating star of spectral type early B or late O with a gaseous circumstellar envelope. In classical Be stars, the circumstellar matter is distributed in a dust-free, ionized Keplerian disk around the star's equator (Rivinius et al. 2013). In BeXB, the main source of matter available for accretion is this circumstellar disk.

HMXBs represent important laboratories to probe physical processes in extreme conditions of gravity and magnetic fields and to study a large number of fundamental astrophysical questions, such as star formation (Grimm et al. 2003; Mineo et al. 2012), masses of neutron stars and their equation of state (van der Meer et al. 2007; Tomsick & Muterspaugh 2010; Manousakis et al. 2012), wind physics (Negueruela 2010) and particle acceleration, including supersonic and relativistic fluid dynamics, emission mechanisms, and radiation reprocessing (Hadrava & Čechura 2012; Bosch-Ramon 2013).

We have been monitoring the HMXBs visible from the Northern Hemisphere in the optical band since 1998. The mon-

itoring consists of *BVRI* photometry and medium resolution spectra around the  $H\alpha$  line. Since 2013, we also obtain polarimetry in the  $R_c$  band. Here we focus on the photometry and present the results of more than ten years worth of observations. In addition to the targets, we obtained standard *BVRI* photometry of a large sample of stars in the HMXBs fields, from which we defined a list of secondary standard stars in the Johnson-Cousins system in each field. Secondary standards will help the monitoring of these objects in the future, as they will allow the obtention of standard photometry without the need of setting up all-sky photometric observing campaigns.

## 2. Observations

The data presented in this work were obtained from the Skinakas Observatory, located in the island of Crete (Greece). Therefore, the list of targets given in Table 1 includes HMXBs that are visible from the Northern Hemisphere (source declination  $\gtrsim -20^\circ$ ). The observations cover the period 2001-2013. We analysed a total of 45 nights. The instrumental set-up consisted of the 1.3 m telescope, the Johnson-Cousins-Bessel (*B*, *V*, *R*, and *I* filters) photometric system (Bessell 1990) and a CCD camera. We employed two different CCD chips. Before 2007 June, a  $1024 \times 1024$  SITE chip with a  $24 \mu\text{m}$  pixel size (corresponding to  $0.5 \text{ arcsec}$  on the sky) was used. From 2007 July, the telescope was equipped with a  $2048 \times 2048$  ANDOR CCD with a  $13.5 \mu\text{m}$  pixel size (corresponding to  $0.28 \text{ arcsec}$  on the sky), and thus providing a field of view of  $\sim 9.5 \text{ arcmin}$  squared.

We carried out a reduction of the data in the standard way, using the IRAF tools for aperture photometry. First, all images were bias-frame subtracted and flat-field corrected using twilight sky flats to correct for pixel-to-pixel variations on the chip. The resulting images are therefore free from the instrumental effects.

Send offprint requests to: pau@physics.uoc.gr

**Table 1.** List of targets.

X-ray name	Optical name	RA (eq. 2000)	DEC (eq. 2000)	Spectral type	$E(B - V)$ (mag.)	Distance (kpc)	disk-loss	X-ray outburst
2S 0114+65	V662 Cas	01 18 02.7	+65 17 30	B1Ia	1.33±0.04	5.9±1.4	–	–
4U 0115+63	V635 Cas	01 18 31.8	+63 44 33	B0.2Ve	1.71±0.05	6.0±1.5	yes	II
IGR J01363+6610	–	01 35 49.5	+66 12 43	B1Ve	1.61±0.03	2.2±0.5	no	–
IGR J01583+6713	–	01 58 18.4	+67 13 23	B2IVe	1.44±0.04	3.4±0.8	no	–
RX J0146.9+6121	LS I +61 235	01 47 00.2	+61 21 24	B1Ve	0.88±0.03	2.5±0.6	no	–
RX J0240.4+6112	LS I +61 303	02 40 31.7	+61 13 46	B0.5Ve	1.09±0.03	1.6±0.4	no	–
V 0332+53	BQ Cam	03 34 59.9	+53 10 23	O8.5Ve	1.94±0.03	6.0±1.5	no	II
RX J0440.9+4431	LS V +44 17	04 40 59.3	+44 31 49	B0.2Ve	0.91±0.03	2.2±0.5	yes	I
1A 0535+262	V725 Tau	05 38 54.6	+26 18 57	O9.7IIIe	0.77±0.04	2.1±0.5	no	I,II
IGR J06074+2205	–	06 07 26.6	+22 05 48	B0.5Ve	0.86±0.03	4.1±1.0	yes	–
AX J1845.0-0433	–	18 45 01.5	–04 33 58	O9Ia	2.42±0.07	5.5±1.5	–	flare
4U 1907+09	–	19 09 37.9	+09 49 49	O9.5Iab	3.31±0.10	4.4±1.2	–	–
XTE J1946+274	–	19 45 39.4	+27 21 56	B0–1IV-Ve	1.18±0.04	7.0±2.0	no	I,II
KS 1947+300	–	19 49 35.5	+30 12 32	B0Ve	2.01±0.05	8.0±2.0	no	I,II
EXO 2030+375	–	20 32 15.3	+37 38 15	B0Ve	3.00±0.20	6.5±2.5	no	I,II
GRO J2058+42	–	20 58 47.5	+41 46 37	O9.5–B0IV-Ve	1.37±0.03	9.0±2.5	no	–
SAX J2103.5+4545	–	21 03 35.7	+45 45 06	B0Ve	1.36±0.03	6.0±1.5	yes	I
IGR J21343+4738	–	21 34 20.4	+47 38 00	B1IV shell	0.75±0.03	10.0±2.5	yes	–
4U 2206+54	BD+53 2790	22 07 56.2	+54 31 06	O9.5Ve	0.51±0.03	3.0±0.7	–	–
SAX J2239.3+6116	–	22 39 20.9	+61 16 27	B0–2III-Ve	1.66±0.04	4.1±1.3	no	–

**Table 2.** Average magnitudes and amplitude of variability of the targets.  $D_j$  is the difference between the largest and smallest measured magnitudes.

Source	$\bar{B}$ (mag)	$\bar{V}$ (mag)	$\bar{R}$ (mag)	$\bar{I}$ (mag)	$D_B$ (mag)	$D_V$ (mag)	$D_R$ (mag)	$D_I$ (mag)	$N_B$	$N_V$	$N_R$	$N_I$
2S 0114+65	12.17	11.03	10.33	9.58	0.17	0.15	0.16	0.09	10	10	10	8
4U 0115+63	16.92	15.34	14.34	13.22	0.67	0.85	1.02	1.04	27	27	27	22
IGR J01363+6610	14.72	13.31	12.32	11.37	0.21	0.16	0.16	0.17	16	16	16	16
IGR J01583+6713	15.71	14.41	13.51	12.66	0.07	0.08	0.08	0.06	9	9	9	9
RX J0146.9+6121	12.09	11.42	11.00	10.52	0.20	0.20	0.18	0.19	26	26	26	20
RX J0240.4+6112	11.61	10.75	10.19	9.55	0.19	0.15	0.12	0.16	11	11	10	10
V 0332+53	17.16	15.42	14.26	13.04	0.28	0.28	0.30	0.35	9	9	9	7
RX J0440.9+4431	11.42	10.73	10.28	9.76	0.18	0.34	0.42	0.48	14	14	14	14
1A 0535+262	9.74	9.19	8.77	8.30	0.27	0.32	0.45	0.44	7	7	7	6
IGR J06074+2205	12.85	12.21	11.80	11.32	0.12	0.27	0.35	0.45	6	6	6	6
AX J1845.0-0433	16.24	14.06	12.71	11.42	0.19	0.11	0.08	0.06	11	11	11	9
4U 1907+09	19.41	16.35	14.40	12.53	0.20	0.18	0.10	0.08	14	14	14	10
XTE J1946+274	18.76	16.92	15.62	14.38	0.31	0.16	0.14	0.11	7	7	7	6
KS 1947+300	15.16	14.22	13.53	12.88	0.14	0.10	0.13	0.13	18	18	18	15
EXO 2030+375	22.16	19.41	17.32	15.18	0.6 <sup>†</sup>	0.23	0.14	0.18	6	8	8	8
GRO J2058+42	16.04	14.89	14.16	13.35	0.21	0.25	0.35	0.44	21	21	21	17
SAX J2103.5+4545	15.34	14.20	13.49	12.75	0.39	0.58	0.70	0.86	21	21	21	18
IGR J21343+4738	14.68	14.16	13.80	13.42	0.23	0.18	0.17	0.12	6	6	6	6
4U 2206+54	10.11	9.84	9.64	9.43	0.19	0.20	0.09	0.13	27	28	27	23
SAX J2239.3+6116	16.26	14.80	13.89	12.92	0.15	0.21	0.28	0.28	7	7	7	7

**Notes.** <sup>(†)</sup> Affected by a large uncertainty due to the faintness of the source in this band.

We took the absorption caused by the Earth’s atmosphere into account with nightly extinction corrections determined from measurements of selected stars that also served as standards. Finally, the photometry was accurately corrected for colour equations and transformed to the standard system using nightly observations of standard stars from Landolt’s catalogue (Landolt 1992,

2009). The linear transformation equations for each filter are of the form

$$m_j^0 = M_j + t_j \times SC + \kappa_j \times X_j + Z_j, \quad (1)$$

where  $m_j^0$  is the atmospheric-extinction-corrected instrumental magnitudes,  $M_j$  the standard value,  $\kappa_j$  is the atmospheric absorp-

tion coefficient,  $X_j$  is the airmass,  $t_j$  a colour coefficient accounting for the differences in spectral response,  $SC$  is a standard star colour, and  $Z_j$  is the zero point of the telescope. The subindex  $j$  runs over different filters. We used  $SC = (B - V)$  as the colour term for the  $B$  and  $V$  filters and  $SC = (V - R)$  and  $SC = (V - I)$  for the  $R$  and  $I$  filters, respectively.

We calculated the error of the photometry in the individual nights as the standard deviation of the difference between the derived final calibrated magnitudes of the standard stars and the magnitudes of the catalogue. Typically errors are of the order of 0.01–0.03 magnitudes.

In general, all the light inside an aperture with radius equal to 16 pixels was summed up to produce the instrumental magnitudes. Because of the presence of near-by objects and larger pixel size of the older CCD, the aperture radius was reduced for XTE J1946+27 and 4U 1907+09. In the case of XTE J1946+27, the aperture radius was taken to be 10 pixels when the ANDOR CCD was used and 8 pixels in observations before 2007. For 4U 1907+09, we used 10 pixels in the observations obtained with the older CCD. We determined the sky background as the statistical mode of the counts inside an annulus 5 pixels wide and 20 pixels from the center of the object.

### 3. Data analysis and selection criteria for secondary standards

Although differential photometry using nearby stars has been performed on some of the targets before (Mendelson & Mazeh 1991; Bell et al. 1993; Finley et al. 1994; Goranskii 2001; Larionov et al. 2001; Baykal et al. 2005; Kızıloğlu et al. 2007; Sarty et al. 2009; Kızıloğlu et al. 2009), this is the first systematic attempt to define secondary standard stars within a few arcminutes of the targets that are suitable for variability studies in a large sample of sources.

The use of comparison stars, i.e. constant stars in the vicinity of the targets, permits differential photometry to be performed. Differential photometry is most suitable to investigate optical photometric variability on short (seconds to minutes) time scales. In addition, if these constant stars have well-determined magnitudes and colours in the standard system, they can be used as local standards to obtain standard photometry of the targets. This approach has a number of advantages with respect to the classical all-sky absolute photometry: it allows us to reach a higher precision; it removes the need to observe standard fields all around the sky, thus saving valuable observing time; it can be performed under less stringent weather conditions; and it eliminates the influence of instrumental drifts, since they affect every star equally.

To find constant stars in the field of view of HMXB, we first extracted the coordinates of a large number of stars using the IRAF task DAOFIND. This task searches for local density maxima, which have a given full-width half-maximum (FWHM) and a peak amplitude greater than a given threshold above the local background. Once the FWHM was fixed, we adjusted the threshold parameter to achieve at least ~40 detections in low-populated fields and ~100 in high-populated fields. Because we obtained the data using different instrumental set-up, the resulting frames differed in orientation and size, making the identification of the same star a time-consuming task. To solve this issue, we calculated the relative position of each star with respect to the target. We converted these relative positions into absolute positions in each frame by adding the coordinates of the target in that frame. Likewise, the image coordinates were scaled down in the smaller

size frames (i.e. observations before 2007) by multiplying by appropriate correction factors.

Instrumental magnitudes were obtained for the target and each of the detections and then transform to the standard system. The final product was the calibrated  $BVRI$  magnitudes as a function of time. Then we derived the average and standard deviation of the data

$$\bar{m}_j = \frac{\sum_{i=1}^{N_j} m_{i,j}}{N_j} \quad (2)$$

$$\sigma_j = \sqrt{\frac{\sum_{i=1}^{N_j} (m_{i,j} - \bar{m}_j)^2}{N_j - 1}}. \quad (3)$$

The index  $j$  represents one of the four filters ( $BVRI$ ) and  $i$  runs over the number of photometric measurements. The quantities  $N_j$  are the total number of good measurements in each filter. In addition, we also calculated the standard deviation of the mean as

$$\sigma_{\bar{m}_j} = \frac{\sigma_j}{\sqrt{N_j}}. \quad (4)$$

Secondary standard stars were selected using the following criteria:

- Variability. Variable stars can be identified as those for which the standard deviation of the measured standard magnitudes is significantly larger than the precision of the standard photometry on individual nights. The standard deviation of the standard photometry is between 0.01 and 0.03 magnitudes for most of the observing nights, as stated above. In addition, measurements of individual stars are also affected by instrumental photometry errors, and by higher photon noise if the star is fainter than the standard stars used to calculate the transformation coefficients. Taking this into account, we consider as non-variable stars those for which the standard deviation (Eq. 3) of the measurements in BVR is less or equal than 0.05 magnitudes. Because the sky is significantly brighter in the  $I$  band, the final magnitudes resulted in slightly larger errors. Thus for the  $I$  band we allowed a larger value of 0.08 magnitudes.
- Number of observations. We rejected stars with fewer than six measurements.
- Colour. The  $(B - V)$  colour index of the comparison stars brackets that of the target object. In most cases, the maximum allowed difference in  $(B - V)$  between the target and the comparison star is 0.5 magnitudes. The only exceptions are 4U 1909+07 and EXO 2030+375, which because of the very high extinction the comparison stars are all bluer than the target.

We imposed no limit on the magnitude of the star. Ideally, the comparison stars should be brighter than the target so that the photon noise of the target dominates that of the standards. This condition is difficult to meet if the target is bright and the field is not very populated. However, for bright objects it does not represent a problem because the secondary standards, although fainter than the target, are bright enough and are photon-noise

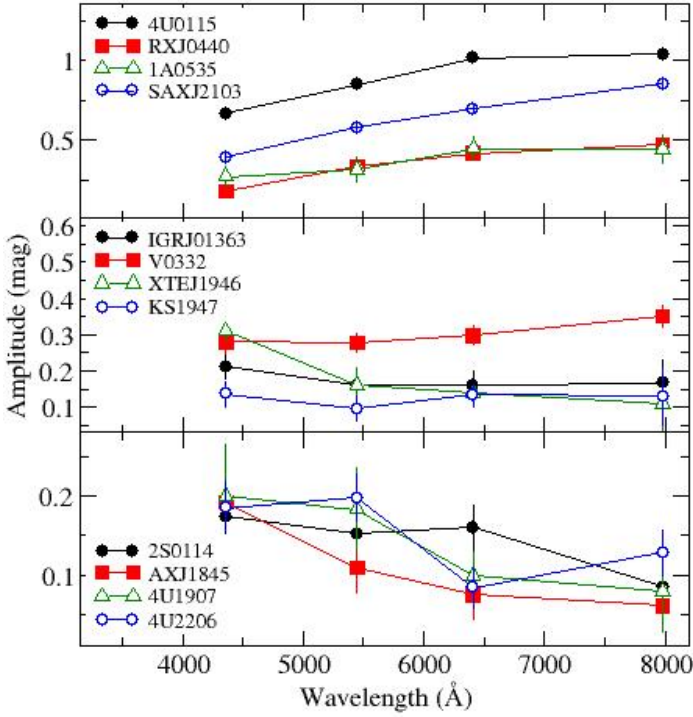


**Fig. 1.** Amplitude of magnitude change as a function of wavelength for BeXB that have gone through disk-loss episodes (upper panel), BeXB with stable disks (middle panel), and SGXB and other wind-fed systems (lower panel).

dominated. For relatively faint targets ( $V_{\text{src}} \gtrsim 14$  mag), the selection criteria generally pick up stars that do not generally differ by more than 1 magnitude from the target value.

The results of our analysis of the field stars are presented in the Appendix. We list a number of stars in the vicinity of the targets that have remained constant over year's time scales. Thus these stars represent good secondary standard stars suitable for calibration purposes and variability studies.

## 4. Results on high-mass X-ray binaries

In this section we present the results of our photometric analysis of the targets. Table 2 lists the results of the observations. In this table, column 1 is the name of the X-ray source. Columns 2–5 contain the mean magnitudes obtained from eq.(2). Columns 6–9 give the difference in magnitude between the maximum and minimum values. Finally, columns 10–13 indicate the number of observations used to derive the mean and the dispersion.

### 4.1. Photometric variability

Be stars are known to display photometric variability on all time scales. While rapid variability is associated with the star's rotation and non-radial pulsations (Balona et al. 2011; Kızıloğlu et al. 2007; Sarty et al. 2009; Gutiérrez-Soto et al. 2011), long-term variability is attributed to structural changes in the circumstellar disk. In BeXBs, the largest amplitude variations are observed on time scales of years (Lyuty & Zaitseva 2000; Reig et al. 2007), which represent the typical time scale for formation and dissipation of the disk (Jones et al. 2008).

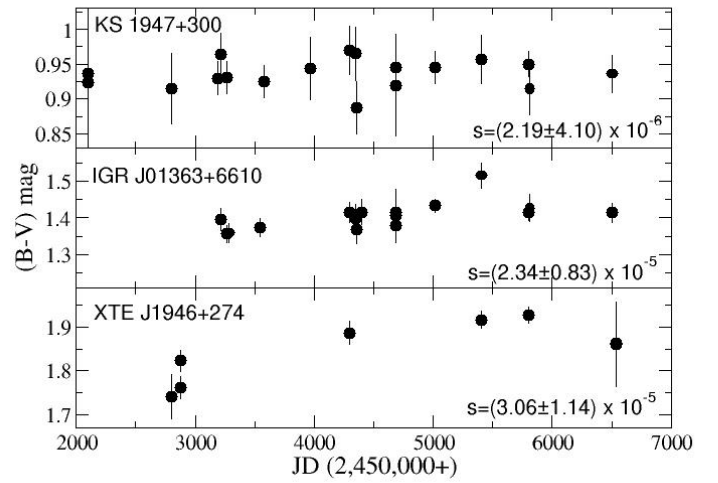


**Fig. 2.** Evolution of the  $(B - V)$  colour index in three BeXB with stable and lasting disks.  $s$  is the slope to a linear fit.

Column 8 in Table 1 indicates whether the systems lost the disk during the interval covered by our observations<sup>1</sup>. By disk-loss episode, we mean that the equivalent width of the  $H\alpha$  line was measured positive, indicating an absorption dominated line. It is possible that a weak and small disk may be present even when emission is not detected (see e.g. Reig & Zezas 2014), but it definitively implies a low optical state.

In general, systems containing Be stars display much larger amplitude of variability in the photometric magnitudes and colours than those harbouring a supergiant companion. In the blue part of the spectrum, where  $\Delta B \lesssim 0.2$  mag, SGXBs tend to be more variable compared to  $\Delta I < 0.1$  mag. In contrast, BeXBs, especially those systems that have gone through episodes of disk dissipation and reformation, such as 4U 0115+63, 1A 0535+262, RX J0440.9+4431, and SAX J2103.5+4545 show the largest magnitude difference in the redder bands with  $\Delta I \gg 0.1$  mag. Note however, that there are BeXBs with stable disks. These systems may show moderate changes in the individual photometric bands, but the colours hardly change on long time scales. These results are illustrated in Figs. 1 and 2. Fig. 1 displays the amplitude of variability as a function of the effective wavelength for the four bandpasses considered for four BeXBs that have gone through disk-loss episodes (upper panel), four BeXB with stable disks (middle panel), four wind-fed systems, three SGXBs, and 4U 2206+54 (lower panel). These three groups of systems exhibit different behaviour. The amplitude of variability in BeXB that have gone through disk-loss episodes increases with wavelength, whereas that in wind-fed systems it decreases. The BeXB with long-lived disks show no obvious trend with wavelength. Fig 2 displays the evolution of the  $(B - V)$  colour index for three BeXB with stable disks. A linear fit to the data shows that the slope is consistent with zero. It is interesting to compare this figure with Fig. 4, where the colour index of two optically variable BeXB is shown and where large amplitude changes are apparent.

The reason for this different behaviour is that while in BeXBs the variability comes from the disk, in supergiant stars it simply reflects the varying but relatively constant (on long time scales) mass-loss rate from the massive companion. The contribution of the disk to the overall continuum emission increases with wave-

<sup>1</sup> 1A 0535+262 went through a disk-loss episode in 1998 (Haigh et al. 1999).

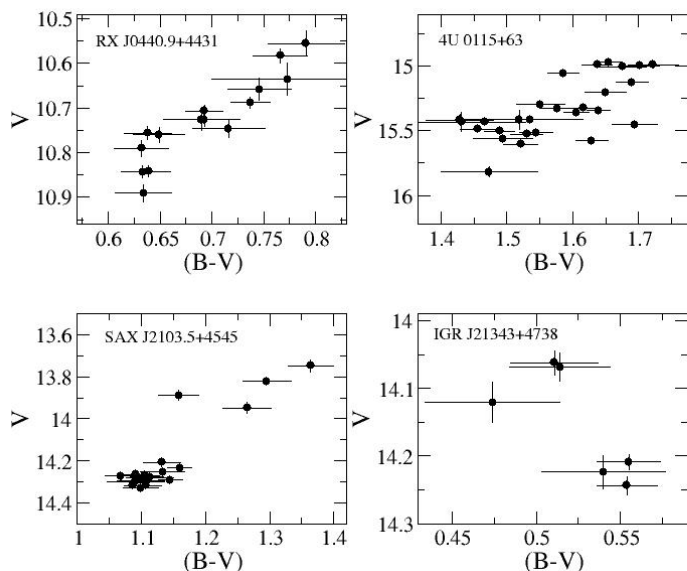


**Fig. 3.**  $(B - V) - V$  colour magnitude diagram for four BeXB that have gone through disk-loss. Note the different behaviour of IGR J21343+4738, the only BeXB with a Be shell companion.

length because the slope of the thermal emission from the photosphere falls much faster than the spectral energy distribution of the free-free radiation (electron bremsstrahlung) from the disk at increasing wavelengths (Gehrz et al. 1974).

Two types of long-term correlated optical photometric and spectroscopic variations have been observed in classical Be stars (Harmanec 2000, 1983). A positive correlation is characterised by an increase in the brightness of the star as the strength of the H I lines increases. In addition, the initial brightening in the optical (e.g.  $V$  band) is accompanied by an increase in the  $(B - V)$  colour. In other words, as the disk reforms after a disk-loss phase, the systems becomes brighter and redder. On the other hand, fewer stars show a negative correlation, that is, the stronger the H $\alpha$  emission, the fainter the star. In this case, the initial fading in the  $V$  band is also accompanied by a reddening of  $(B - V)$ . These correlations are attributed to a geometrical effect (Harmanec 1983). Stars viewed at very high inclination angles show the inverse correlation, whereas stars seen at certain inclination angles  $i < i_{\text{crit}}$ , exhibit the positive correlation. At very high inclination angles (equator-on stars), the inner parts of the Be envelope partly block the stellar photosphere, while the small projected area of the disk on the sky keeps the disk emission to a minimum. In stars not seen equator-on, the effect of the disk is to increase the effective radius of the star: as the disk grows an overall (star plus disk) increase in brightness is expected. The value of the critical inclination angle is not known, but a rough estimate based on available data suggest  $i_{\text{crit}} \sim 75^\circ$  (Sigut & Patel 2013).

Figure 3 shows four BeXB that have gone through a disk-loss phase. The Be companion in IGR J21343+4738 is the only shell star of the four (Reig & Zezas 2014). The presence of shell absorption lines indicate that the line of sight to the star lies nearly perpendicular to its rotation axis. While most of the BeXB show the positive correlation between  $V$  and  $(B - V)$ , IGR J21343+4738 shows the negative correlation, hence confirming Harmanec (1983) explanation. The inverse correlation has been questioned by Haubois et al. (2012) who argued that the changes of  $(B - V)$  in shell stars should be of rather small amplitude. Large change of the  $(B - V)$  colour in this case might be due to other causes, such as  $V/R$  variations, rather than to mass

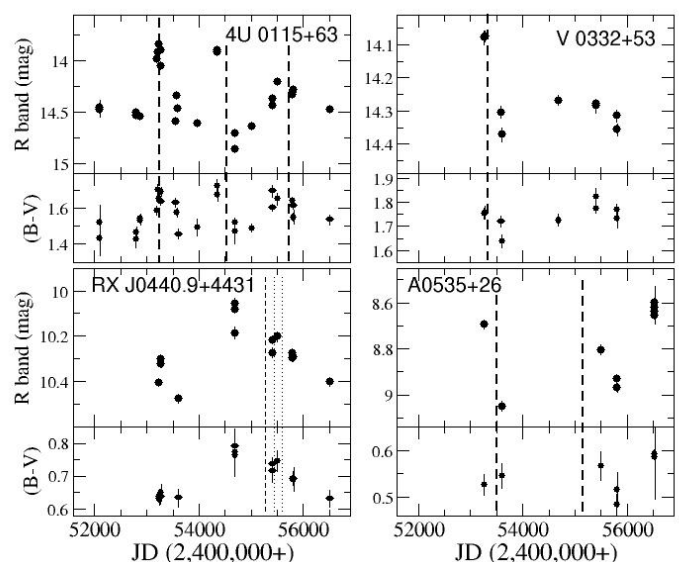


**Fig. 4.**  $R$ -band and  $(B - V)$  light curves of four BeXB displaying large amplitude X-ray activity. The dashed and dotted vertical lines indicate the epochs when type II and type I X-ray outbursts occurred, respectively. A decrease in the optical brightness following the outburst is seen in all systems.

injection. The current data on IGR J21343+4738 show indeed a much smaller change in  $(B - V)$  with respect to the other three sources. However, this may simply because of the fact that the disk growth is still in the initial phase in this system as indicated by the weak H $\alpha$  emission (Reig & Zezas 2014).

#### 4.2. Colour excess and distance

In Be stars, the total measured reddening is made up of two components: one produced mainly by dust in the interstellar space through the line of sight and another produced by the circumstellar gas around the Be star (Dachs et al. 1988; Fabregat & Reglero 1990). Although the physical origin and wavelength dependence of these two reddenings is completely different, their final effect upon the colours is very difficult to disentangle (Torrejón et al. 2007). Indeed, interstellar reddening is caused by "absorption" and "scattering" processes, while circumstellar reddening is due to extra "emission" at longer wavelengths. In this respect, disk-loss episodes are extremely important because they allow us to derive the true magnitudes and colours of the underlying Be star, without the contribution of the disk.

The colour excess is simply  $E(B - V) = (B - V)_{\text{obs}} - (B - V)_0$ , where  $(B - V)_{\text{obs}}$  is the observed colour and  $(B - V)_0$  the intrinsic colour. To minimise the contribution of the disk, we used the data with the bluest colour index of each target. The colour excess of the sources considered in this work is listed in Table 1.

The uncertainty in estimating the distance stems from the uncertainty of the spectral classification and of the intrinsic colour and absolute magnitude calibrations. In particular, the error associated with the absolute magnitude calibration can be large (Jaschek & Gómez 1998; Wegner 2006). We estimate the intrinsic colour and absolute magnitude from the spectral type given in Table 1. The adopted  $(B - V)_0$  colour is the average of the values from Johnson (1966), Fitzgerald (1970), Gutierrez-Moreno (1979), and Wegner (1994) and the associated error, the standard deviation. The absolute magnitude was taken from Wegner (2006), who gives different calibrations for emitting and non-

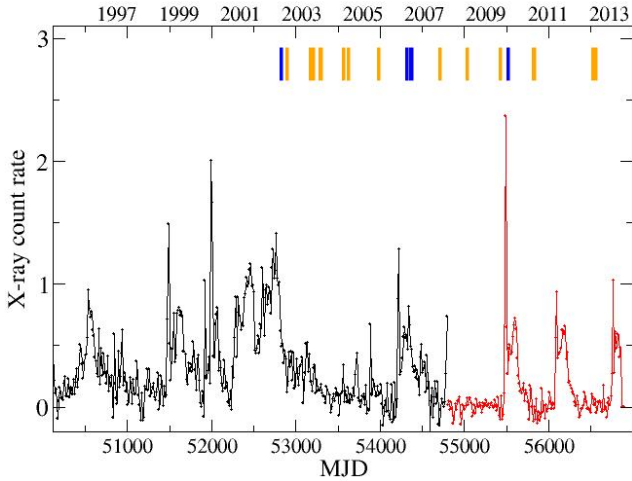


**Fig. 5.** Long-term X-ray variability of SAX J2103.5+4545 as seen by the all-sky monitors *RXTE*/ASM (black) and *Swift*/BAT light curves (red). The original one-day resolution light curves were rebinned to a bin size equal to the orbital period ( $P_{\text{orb}} = 12.67$  d). The blue and orange vertical lines indicate the epochs when the *BVRI* magnitudes were below (brighter) and above (fainter) the average, respectively.

emitting B stars. For the error in  $M_V$ , we assumed 0.5 magnitudes. Only for the systems where the spectral type is not well constrained we took 0.6 magnitudes. The error in the distance was then obtained by propagating the errors in  $V$ ,  $E(B - V)$ ,  $(B - V)_0$ , and  $M_V$ . Typically, the error in the distance given in Table 1 is  $\sim 25\%$ .

#### 4.3. Correlated X-ray/optical variability

Because the disk constitutes the main reservoir of matter available for accretion, a correlation between X-rays and optical emission should be expected. Although on short time scales (days-weeks, sometimes even months) the relationship between optical emission and X-rays is complex and not always seen, when one considers time scales of years, the correlation is generally observed. The correlation identifies the circumstellar disk as the main source of optical and X-ray variability.

The material in the disk is the fuel that powers the X-rays through accretion. The system shines bright in X-rays while there is enough fuel. When this is exhausted the X-rays switch off. This is illustrated in Fig. 4, where a significant decline in the optical brightness is observed after the occurrence of X-ray outbursts. Figure 5 shows the long-term X-ray light curve of SAX J2103.5+4545 using the all-sky monitors on board *RXTE* and *Swift*<sup>2</sup>. The vertical blue and orange lines correspond to observations in which the photometric magnitudes were below (brighter) and above (fainter) the average, respectively (see Table 2). Clearly, low-intensity optical states are seen during faint X-ray states, whereas during bright X-ray states the source displays brighter optical magnitudes.

Sometimes the source may be active in X-rays for a very long time even after a major X-ray outburst, however, the X-rays cease once the matter supply ends. An example of this behaviour

<sup>2</sup> To bring the BAT data points to the same scale as the ASM data points, we multiply the BAT data by 129.3. This constant was derived by taking into account the correspondence between intensity (mCrab) and count rate of the two instruments (1 mCrab corresponds to 0.075 ASM count  $\text{s}^{-1}$  and to 0.00022 BAT count  $\text{cm}^{-2} \text{s}^{-1}$ ) and the fact that the Crab emits about 38% more in the 2–10 keV than in the 15–50 keV band.

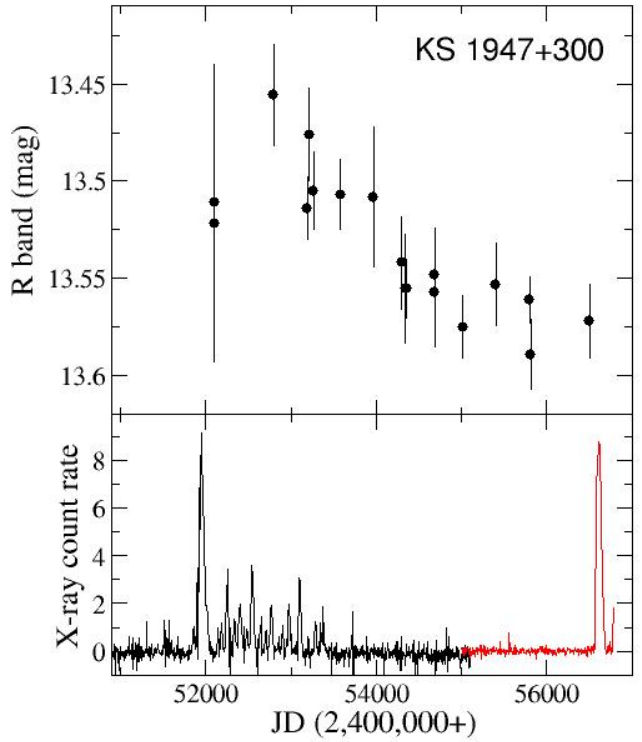


**Fig. 6.** *R*-band and X-ray light curves of KS 1947+300 from the *RXTE*/ASM (black) and *Swift*/BAT (red) all-sky monitors. Note the longer disk variability time-scales (changes in the optical brightness) with respect to systems shown in Fig. 4.

can be seen in Fig. 6, where the optical (*R*-band) and X-ray light curves of KS 1947+300 are shown. The X-ray data come from the all-sky monitors *RXTE*/ASM (2–10 keV) for observation before MJD 55000 and from *Swift*/BAT (15–50 keV) after that date. During the  $\sim$  five years that KS 1947+300 was active in X-rays ( $\sim$  MJD 51900–53500), the optical brightness remained fairly constant at  $R \sim 13.5$  magnitudes. After MJD 53500, *R* decreased and the X-ray activity ceased. For the next  $\sim$  eight years the optical brightness did not vary significantly ( $R = 13.56 \pm 0.01$ ) and the system remained in an off X-ray state. Surprisingly, the source went into another outburst without a substantial rebrightening in the optical magnitudes.

Historically, the long-term X-ray variability of BeXB has been characterised by two type of outbursts.

- Type I outbursts are regular and (quasi-)periodic outbursts, normally peaking at or close to periastron passage of the neutron star. They are short-lived, i.e. tend to cover a relatively small fraction of the orbital period (typically  $0.2\text{--}0.3 P_{\text{orb}}$ ). The X-ray flux increases by up to two orders of magnitude with respect to the pre-outburst state, reaching peak luminosities  $L_X \lesssim 10^{37} \text{ erg s}^{-1}$ . The number of detected type I outbursts varies from source to source, but typically the source remains active for 3–8 periastron passages. A remarkable case is EXO 2030+375, which shows type I outbursts almost permanently.
- Type II outbursts represent major increases of the X-ray flux,  $10^3 - 10^4$  times that at quiescence. They may reach the Eddington luminosity for a neutron star ( $L_X \sim 10^{38} \text{ erg s}^{-1}$ ) and become the brightest objects of the X-ray sky. They do not show any preferred orbital phase and last for a large fraction of an orbital period or even for several orbital periods.

Column 9 in Table 1 indicates the type of outburst detected during the course of our observation in the interval 2001–2013.



It should be emphasized that as X-ray missions generate more data, it has become apparent that classification based solely on the X-ray luminosity is too simplistic. Outbursts in BeXB show a large variety of properties and many outbursts do not always follow this simple scheme (Kretschmar et al. 2012).

In principle, a type II outburst appears as a dramatic event that may lead to the dissipation of the disk. In practice, the loss of the disk after a major outburst is the exception rather than the rule. Of the systems that exhibited type II outbursts, only 4U 0115+63 loses the disk after major outbursts (Reig et al. 2007). Nevertheless, type II outbursts do affect the structure of the disk (Fig. 4) and fainter optical emission is generally detected after such events.

Although estimating the total mass contained in a disk is rather uncertain because of the uncertainty in its size and density, an order of magnitude calculation of the amount of material that is accreted in the two cases would be illustrative. To generate an average  $L_X \sim 1 \times 10^{37}$  erg s<sup>-1</sup> over 100 days, a mass accretion rate of  $\dot{M} \sim 2.7 \times 10^{17}$  g s<sup>-1</sup> is needed. Assuming that all the potential energy loss in the accretion process is converted in radiation,  $\dot{M} = L_X(R/GM)$ , then the total amount of matter accreted into the neutron star is  $4.7 \times 10^{23}$  g. In the case of a type I outburst with average luminosity,  $L_X \sim 3 \times 10^{35}$  erg s<sup>-1</sup>, and a duration of 20 days, the total accreted mass would be  $2.8 \times 10^{21}$  g.

The total mass of the disk can be computed as  $M = \int \rho dV$ , with  $\rho = \rho_0(R_*/r)^n$  and  $dV = 2\pi r H dr$ . Here  $\rho_0$  is the density and the inner radius of the disk (at  $r \sim R_*$ ),  $R_*$  the star radius,  $H$  the disk height, and  $n$  an exponent defining the density law. The parameter  $n$  varies in the range 3–3.5 in most BeX (Waters et al. 1988). The typical radius of a B0V star, is  $R_* = 8 R_\odot$  and assuming typical values for the disk radius  $R_d = 5R_*$ , and inner density  $\rho_0 = 10^{-10}$  g cm<sup>-3</sup> (Telting et al. 1998) and  $H = 0.03R_*$  (Negueruela & Okazaki 2001) the mass is estimated to be  $2 \times 10^{24}$  g.

Therefore, while in a type II outburst the total accreted mass may represent an important part of the disk, only an insignificant 0.1% of the total mass is accreted onto the neutron star during the course of a type I outburst. Even if the outbursts are repeated several times, the disk may not be substantially affected.

## 5. Summary and conclusion

We have studied the long-term optical photometric variability of the counterparts to high-mass X-ray binaries visible from the Northern Hemisphere. Our results can be summarised as follows:

1. There is a complex connection between the optical and X-ray variability in BeXB. However, when time-scales of years are considered, there is a correlation between the long-term evolution of the system optical brightness and the X-ray activity. After a major X-ray outburst the optical magnitudes are always fainter than before the outburst.
2. The disk is the main source of optical variability because the disk itself emits at these wavelength, but it is also responsible for the X-ray variability because it constitutes the source of matter available for accretion. As long as the disk is stable, no changes are seen in the colour indices. In BeXB with stable disks, the amplitude change in magnitudes shows almost no variation with wavelength.
3. The more variable the BeXB in the optical band, the more variable in the X-ray band. Systems with the larger amplitude of variability in the optical magnitudes and colours are

those with also the larger amplitude changes in the X-ray band.

4. The HMXB with Be companions display larger amplitude of optical variability ( $\Delta V \gg 0.1$  mag) than SGXBs ( $\Delta V \lesssim 0.1$  mag).
5. The amplitude of variability increases with wavelength in BeXB with fast-changing disks and decreases in SGXBs.
6. The positive and negative (or inverse) correlations between luminosity and colour during disk growth observed in classical Be stars are also present in BeXBs.
7. Contrary to general belief, type II outbursts do not generally lead to the total destruction of the disk, although in some cases, such as in 4U 0115+63, it does lead to the total destruction of the disk. In this system, the optical variability can be explained by a build up and disruption of the circumstellar disk on times scales of three–five years.
8. We have also set up a list of secondary standard stars in the field of view of high-mass X-ray binaries. This work can benefit observers who seek to perform differential photometry for frequency analysis. It also allows us to perform standard photometry without the framework of a full all-sky absolute photometry observing campaign.

*Acknowledgements.* The work of J.F. is supported by the Spanish Ministerio de Economía y Competitividad, and FEDER, under contract AYA2010-18352. P.R. and J.F. are partially supported by the Generalitat Valenciana project of excellence PROMETEOII/2014/060. Skinakas Observatory is a collaborative project of the University of Crete and the Foundation for Research and Technology-Hellas. This work made use of NASA's Astrophysics Data System Bibliographic Services and of the SIMBAD database, operated at the CDS, Strasbourg, France. PR acknowledges partial help from the COST action MP1304 "Exploring fundamental physics with compact stars".

## References

- Balona, L. A., Pigulski, A., Cat, P. D., et al. 2011, MNRAS, 413, 2403  
 Baykal, A., Kızıloğlu, Ü., Kızıloğlu, N., Balman, Ş., & Inam, S. Ç. 2005, A&A, 439, 1131  
 Bell, S. A., Hilditch, R. W., & Pollacco, D. L. 1993, MNRAS, 265, 1042  
 Bessell, M. S. 1990, PASP, 102, 1181  
 Bonnarel, F., Fernique, P., Bienaymé, O., et al. 2000, A&AS, 143, 33  
 Bosch-Ramon, V. 2013, A&A, 560, A32  
 Dachs, J., Kiehling, R., & Engels, D. 1988, A&A, 194, 167  
 Fabregat, J. & Reglero, V. 1990, MNRAS, 247, 407  
 Finley, J. P., Taylor, M., & Belloni, T. 1994, ApJ, 429, 356  
 Fitzgerald, M. P. 1970, A&A, 4, 234  
 Gehrz, R. D., Hackwell, J. A., & Jones, T. W. 1974, ApJ, 191, 675  
 Goranskii, V. P. 2001, Astronomy Letters, 27, 516  
 Grimm, H.-J., Gilfanov, M., & Sunyaev, R. 2003, MNRAS, 339, 793  
 Gutierrez-Moreno, A. 1979, PASP, 91, 299  
 Gutiérrez-Soto, J., Reig, P., Fabregat, J., & Fox-Machado, L. 2011, in IAU Symposium, Vol. 272, IAU Symposium, ed. C. Neiner, G. Wade, G. Meynet, & G. Peters, 505–506  
 Hadrava, P. & Čechura, J. 2012, A&A, 542, A42  
 Haigh, N. J., Coe, M. J., Steele, I. A., & Fabregat, J. 1999, MNRAS, 310, L21  
 Harmanec, P. 1983, Hvar Observatory Bulletin, 7, 55  
 Harmanec, P. 2000, in Astronomical Society of the Pacific Conference Series, Vol. 214, IAU Colloq. 175: The Be Phenomenon in Early-Type Stars, ed. M. A. Smith, H. F. Henrichs, & J. Fabregat, 13  
 Haubois, X., Carciofi, A. C., Rivinius, T., Okazaki, A. T., & Bjorkman, J. E. 2012, ApJ, 756, 156  
 Jaschek, C. & Gómez, A. E. 1998, Highlights of Astronomy, 11, 566  
 Johnson, H. L. 1966, ARA&A, 4, 193  
 Jones, C. E., Sigut, T. A. A., & Porter, J. M. 2008, MNRAS, 386, 1922  
 Kızıloğlu, Ü., Kızıloğlu, N., Baykal, A., Yerli, S. K., & Özbey, M. 2007, A&A, 470, 1023  
 Kızıloğlu, Ü., Özbilgen, S., Kızıloğlu, N., & Baykal, A. 2009, A&A, 508, 895  
 Kretschmar, P., Nespoli, E., Reig, P., & Anders, F. 2012, in Proceedings of "An INTEGRAL view of the high-energy sky (the first 10 years)" - 9th INTEGRAL Workshop and celebration of the 10th anniversary of the launch (INTEGRAL 2012). 15-19 October 2012. Bibliotheque Nationale de France, Paris, France. Published online at <A href="http://pos.sissa.it/cgi-bin/reader/conf.cgi?confid=176">http://pos.sissa.it/cgi-bin/reader/conf.cgi?confid=176</A>, id.16

- Landolt, A. U. 1992, *AJ*, 104, 340
- Landolt, A. U. 2009, *AJ*, 137, 4186
- Larionov, V., Lyuty, V. M., & Zaitseva, G. V. 2001, *A&A*, 378, 837
- Lyuty, V. M. & Zaitseva, G. V. 2000, *Astronomy Letters*, 26, 9
- Manousakis, A., Walter, R., & Blondin, J. M. 2012, *A&A*, 547, A20
- Mendelson, H. & Mazeh, T. 1991, *MNRAS*, 250, 373
- Mineo, S., Gilfanov, M., & Sunyaev, R. 2012, *MNRAS*, 419, 2095
- Negueruela, I. 2010, in *Astronomical Society of the Pacific Conference Series*, Vol. 422, *High Energy Phenomena in Massive Stars*, ed. J. Martí, P. L. Luque-Escamilla, & J. A. Combi, 57
- Negueruela, I. & Okazaki, A. T. 2001, *A&A*, 369, 108
- Reig, P., Larionov, V., Negueruela, I., Arkharov, A. A., & Kudryavtseva, N. A. 2007, *A&A*, 462, 1081
- Reig, P. & Zezas, A. 2014, *A&A*, 561, A137
- Rivinius, T., Carciofi, A. C., & Martayan, C. 2013, *A&A Rev.*, 21, 69
- Sarty, G. E., Kiss, L. L., Huziak, R., et al. 2009, *MNRAS*, 392, 1242
- Sigut, T. A. A. & Patel, P. 2013, *ApJ*, 765, 41
- Telting, J. H., Waters, L. B. F. M., Roche, P., et al. 1998, *MNRAS*, 296, 785
- Tomsick, J. A. & Muterspaugh, M. W. 2010, *ApJ*, 719, 958
- Torrejón, J. M., Negueruela, I., & Riquelme, M. S. 2007, in *Astronomical Society of the Pacific Conference Series*, Vol. 361, *Active OB-Stars: Laboratories for Stellar and Circumstellar Physics*, ed. A. T. Okazaki, S. P. Owocki, & S. Stefl, 503
- van der Meer, A., Kaper, L., van Kerkwijk, M. H., Heemskerk, M. H. M., & van den Heuvel, E. P. J. 2007, *A&A*, 473, 523
- Waters, L. B. F. M., van den Heuvel, E. P. J., Taylor, A. R., Habets, G. M. H. J., & Persi, P. 1988, *A&A*, 198, 200
- Wegner, W. 1994, *MNRAS*, 270, 229
- Wegner, W. 2006, *MNRAS*, 371, 185

## Appendix A: Secondary standard stars

Table A.1 to A.5 list the final set of secondary standard stars for each target. In these tables, column 5 gives the angular distance between the star and the target. Columns 6–9 are the mean magnitudes, columns 10–13 show the standard deviation of the mean calculated from eq. (4) and columns 14–17 show the number of measurements considered. The RA and DEC and the angular distance from the target to the secondary standards were derived using the ALADIN Sky Atlas (Bonnarel et al. 2000).

Finding charts with the identification of the secondary standard stars are also available in electronic form at the CDS through the Vizier service <http://vizier.u-strasbg.fr/viz-bin/VizieR>.



**Table A.1.** Secondary standards in the field of view of high-mass X-ray binaries. The mean and standard deviation of the mean in the *BVR* bands (calculated from eqs. (2) and (4)) and the number of observations are given.

Star	ID	RA	DEC	d (')	$\bar{B}$ (mag)	$\bar{V}$ (mag)	$\bar{R}$ (mag)	$\bar{I}$ (mag)	$\sigma_{\bar{B}}$ (mag)	$\sigma_{\bar{V}}$ (mag)	$\sigma_{\bar{R}}$ (mag)	$\sigma_{\bar{I}}$ (mag)	$N_B$	$N_V$	$N_R$	$N_I$
2S 0114+65																
C1	9	01 18 19.3	+65 20 28	3.4	14.908	13.903	13.274	12.629	0.017	0.004	0.008	0.016	9	9	9	7
C2	26	01 17 29.4	+65 17 06	3.5	11.933	11.256	10.877	10.419	0.006	0.009	0.004	0.006	10	10	10	8
C3	36	01 17 31.9	+65 15 59	3.6	15.370	13.991	13.095	12.318	0.013	0.011	0.008	0.008	10	10	10	8
C4	47	01 17 54.7	+65 14 36	3.0	13.846	13.029	12.546	12.091	0.008	0.005	0.005	0.006	10	10	10	8
4U 0115+63																
C1	7	01 18 45.6	+63 47 57	3.7	16.606	15.397	14.682	14.040	0.011	0.008	0.007	0.006	22	22	22	17
C2	8	01 18 19.2	+63 47 56	3.6	14.629	13.755	13.255	12.708	0.008	0.008	0.007	0.006	22	22	22	18
C3	9	01 18 58.9	+63 47 53	4.4	17.095	15.829	15.092	14.337	0.009	0.008	0.008	0.008	22	23	22	18
C4	10	01 18 46.9	+63 47 49	3.6	16.734	15.358	14.541	13.605	0.007	0.008	0.008	0.008	22	23	23	18
C5	12	01 18 16.6	+63 47 38	3.5	16.583	15.440	14.768	14.089	0.008	0.007	0.008	0.007	22	23	23	19
C6	15	01 18 31.4	+63 47 29	2.9	16.332	15.066	14.337	13.470	0.008	0.008	0.007	0.007	22	23	24	18
C7	32	01 18 46.4	+63 46 03	2.1	16.121	14.612	13.711	12.699	0.008	0.008	0.007	0.008	23	25	24	21
C8	54	01 18 57.7	+63 44 59	2.8	14.347	13.535	13.108	12.561	0.007	0.008	0.007	0.004	22	23	23	17
C9	62	01 18 49.2	+63 44 22	2.0	15.464	14.440	13.853	13.195	0.007	0.008	0.007	0.005	24	25	25	20
C10	67	01 18 45.1	+63 44 04	1.5	13.737	13.005	12.619	12.127	0.011	0.009	0.009	0.007	18	17	18	13
C11	98	01 18 10.8	+63 41 44	3.6	17.142	15.934	15.231	14.398	0.008	0.008	0.008	0.008	22	25	25	21
IGR J01363+6610																
C1	12	01 36 20.6	66 15 34	4.1	17.101	15.281	14.221	13.192	0.014	0.008	0.005	0.009	11	11	11	11
C2	13	01 36 09.6	66 15 17	3.2	16.060	14.806	14.071	13.338	0.011	0.004	0.004	0.005	12	11	12	12
C3	17	01 36 20.5	66 14 41	3.6	16.271	15.017	14.265	13.457	0.010	0.008	0.006	0.004	12	13	13	12
C4	18	01 36 28.1	66 14 31	4.2	15.246	13.375	12.287	11.255	0.013	0.011	0.008	0.007	12	13	13	12
C5	75	01 35 53.2	66 11 27	1.2	16.284	14.877	14.068	13.311	0.009	0.006	0.004	0.006	16	15	15	15
C6	82	01 36 20.4	66 10 14	3.9	15.743	14.582	13.895	13.196	0.010	0.007	0.006	0.008	14	14	14	14
C7	87	01 35 34.6	66 09 25	3.6	16.808	15.340	14.366	13.422	0.012	0.005	0.005	0.008	16	15	15	15
C8	90	01 35 18.5	66 08 38	5.1	14.361	13.191	12.541	11.920	0.011	0.005	0.005	0.004	13	12	12	12
IGR J01583+6713																
C1	23	01 58 22.3	+67 14 33	1.2	17.743	16.369	15.553	14.814	0.014	0.008	0.008	0.009	9	9	9	9
C2	24	01 58 20.0	+67 14 29	1.1	16.192	14.886	14.094	13.315	0.014	0.005	0.006	0.006	9	9	9	9
C3	28	01 57 55.7	+67 13 58	2.2	16.299	14.871	14.019	13.119	0.014	0.005	0.006	0.005	9	9	9	9
C4	29	01 57 45.1	+67 13 48	3.2	17.546	16.240	15.473	14.605	0.015	0.004	0.006	0.004	9	9	9	9
C5	55	01 58 30.9	+67 13 20	1.2	16.039	14.682	13.863	13.144	0.015	0.013	0.013	0.013	9	9	9	9
C6	85	01 58 30.9	+67 10 35	3.0	15.361	13.992	13.201	12.339	0.010	0.005	0.005	0.005	9	9	9	9
C7	90	01 57 47.4	+67 10 06	4.4	16.960	15.589	14.658	13.863	0.014	0.005	0.006	0.006	9	9	9	9
C8	93	01 58 24.8	+67 10 03	3.3	17.782	16.254	15.206	13.780	0.015	0.006	0.006	0.005	9	9	9	9

**Table A.2.** Secondary standards in the field of view of high-mass X-ray binaries (cont.)

Star	ID	RA	DEC	d (')	$\bar{B}$ (mag)	$\bar{V}$ (mag)	$\bar{R}$ (mag)	$\bar{I}$ (mag)	$\sigma_{\bar{B}}$ (mag)	$\sigma_{\bar{V}}$ (mag)	$\sigma_{\bar{R}}$ (mag)	$\sigma_{\bar{I}}$ (mag)	$N_B$	$N_V$	$N_R$	$N_I$
RX J0146.9+6121																
C1	9	01 47 30.0	+61 25 18	5.3	12.623	12.041	11.676	11.315	0.007	0.004	0.005	0.007	18	17	17	15
C2	12	01 47 39.4	+61 24 43	4.2	14.033	13.061	12.506	11.975	0.006	0.007	0.006	0.005	20	23	21	18
C3	13	01 47 19.6	+61 24 23	3.8	14.174	13.381	12.938	12.434	0.006	0.006	0.005	0.005	22	22	22	17
C4	14	01 47 30.4	+61 23 14	4.0	13.250	12.608	12.226	11.780	0.007	0.006	0.006	0.005	20	20	20	17
C5	16	01 47 22.5	+61 23 07	3.2	14.713	13.710	13.131	12.483	0.007	0.007	0.005	0.006	22	22	22	19
C6	24	01 47 15.2	+61 22 12	1.9	13.525	12.900	12.525	12.092	0.006	0.006	0.005	0.003	24	24	24	18
C7	34	01 46 32.6	+61 21 18	3.3	12.496	11.681	11.211	10.652	0.006	0.005	0.006	0.004	23	23	23	20
C8	35	01 47 22.8	+61 21 02	2.6	11.388	10.841	10.512	10.123	0.008	0.005	0.005	0.004	22	20	21	17
C9	39	01 46 51.6	+61 20 54	1.1	14.532	13.736	13.255	12.750	0.007	0.005	0.006	0.004	25	25	24	20
C10	48	01 46 47.7	+61 20 09	1.8	12.295	11.501	11.042	10.509	0.007	0.004	0.005	0.004	25	23	24	19
C11	53	01 46 51.4	+61 19 28	2.1	13.028	12.348	11.944	11.543	0.006	0.003	0.005	0.005	24	22	24	20
C12	55	01 47 20.9	+61 19 10	3.2	14.057	13.377	13.001	12.529	0.008	0.006	0.006	0.005	26	23	24	20
C13	64	01 47 09.5	+61 18 42	2.8	13.577	12.568	11.995	11.444	0.008	0.005	0.005	0.005	25	24	23	20
C14	78	01 47 23.8	+61 17 45	4.5	14.904	13.912	13.368	12.734	0.011	0.006	0.009	0.012	22	19	21	18
C15	85	01 46 41.9	+61 27 14	4.6	13.591	12.981	12.619	12.188	0.010	0.009	0.010	0.004	14	14	14	12
RX J0240.4+6112																
C1	35	02 40 43.6	+61 16 21	2.8	13.450	12.875	12.547	12.141	0.012	0.012	0.010	0.024	8	8	8	8
C2	39	02 40 51.0	+61 15 45	2.9	12.177	11.615	11.274	10.888	0.005	0.009	0.007	0.014	9	10	10	9
C3	41	02 40 35.1	+61 15 37	1.8	14.016	13.345	12.947	12.475	0.009	0.010	0.011	0.013	10	11	10	10
C4	45	02 39 59.1	+61 15 19	4.2	11.151	10.798	10.604	10.341	0.011	0.009	0.009	0.012	10	10	9	9
C5	47	02 40 24.1	+61 15 14	1.7	15.032	14.244	13.812	13.289	0.012	0.010	0.008	0.006	11	11	10	10
C6	59	02 40 13.1	+61 13 39	2.1	13.821	12.869	12.324	11.746	0.008	0.011	0.011	0.014	10	11	10	10
C7	64	02 40 35.7	+61 12 43	1.1	13.171	12.392	11.957	11.426	0.007	0.009	0.006	0.007	10	11	10	10
C8	72	02 40 55.8	+61 11 20	3.7	14.103	13.322	12.873	12.401	0.009	0.012	0.009	0.012	9	9	9	8
C9	80	02 39 57.4	+61 10 48	5.0	16.129	15.146	14.600	13.989	0.012	0.008	0.009	0.012	9	10	9	10
C10	81	02 40 10.7	+61 10 45	3.8	14.571	13.901	13.514	13.077	0.006	0.009	0.011	0.016	10	11	10	10
C11	84	02 39 57.1	+61 10 28	5.2	15.088	14.180	13.637	13.079	0.016	0.010	0.011	0.009	10	10	9	10
C12	86	02 40 49.5	+61 10 25	3.9	14.678	13.393	12.675	11.970	0.008	0.012	0.012	0.010	10	11	10	10
V 0332+53																
C1	27	03 34 37.2	+53 12 28	3.9	17.966	16.395	15.472	14.538	0.013	0.012	0.013	0.007	9	9	9	7
C2	32	03 35 03.7	+53 12 09	1.7	14.908	13.790	13.128	12.477	0.011	0.012	0.010	0.004	9	9	9	7
C3	34	03 34 52.9	+53 11 53	1.7	16.425	14.897	13.979	13.045	0.009	0.010	0.010	0.006	9	9	9	7
C4	45	03 34 36.6	+53 10 23	3.4	17.035	15.632	14.813	13.973	0.015	0.011	0.012	0.007	9	9	9	7
C5	48	03 34 50.1	+53 09 58	1.5	16.924	15.493	14.522	13.417	0.012	0.014	0.013	0.008	9	9	9	7
C6	57	03 34 40.9	+53 08 36	3.3	16.861	15.240	14.225	13.140	0.013	0.010	0.009	0.008	9	9	9	7

**Table A.3.** Secondary standards in the field of view of high-mass X-ray binaries (cont.)

Star	ID	RA	DEC	d (')	$\bar{B}$ (mag)	$\bar{V}$ (mag)	$\bar{R}$ (mag)	$\bar{I}$ (mag)	$\sigma_{\bar{B}}$ (mag)	$\sigma_{\bar{V}}$ (mag)	$\sigma_{\bar{R}}$ (mag)	$\sigma_{\bar{I}}$ (mag)	$N_B$	$N_V$	$N_R$	$N_I$
RX J0440.9+4431																
C1	3	04 41 05.0	+44 34 39	3.0	15.503	14.437	13.740	12.905	0.012	0.013	0.012	0.004	13	13	13	11
C2	4	04 40 45.1	+44 34 12	3.4	13.410	12.334	11.710	11.093	0.007	0.009	0.007	0.004	13	13	13	12
C3	6	04 41 25.0	+44 33 25	4.8	15.550	14.426	13.751	13.040	0.016	0.014	0.016	0.008	8	8	8	8
C4	7	04 40 54.9	+44 33 18	1.6	14.879	13.926	13.367	12.757	0.007	0.012	0.011	0.009	15	15	15	14
C5	9	04 40 43.4	+44 32 29	2.8	15.665	14.625	14.022	13.403	0.012	0.010	0.010	0.009	14	14	14	13
C6	12	04 40 35.6	+44 32 04	4.2	15.688	14.738	14.181	13.587	0.010	0.015	0.004	0.009	10	10	10	9
C7	13	04 40 37.3	+44 31 58	3.8	14.524	13.758	13.315	12.800	0.010	0.012	0.009	0.010	12	12	12	11
C8	18	04 40 40.9	+44 31 24	3.2	14.707	13.696	13.089	12.437	0.006	0.008	0.008	0.006	13	13	13	12
C9	19	04 40 35.9	+44 31 18	4.0	15.454	14.504	13.927	13.323	0.008	0.012	0.009	0.005	12	12	12	10
C10	20	04 40 39.2	+44 31 04	3.6	15.560	14.818	14.400	13.884	0.013	0.012	0.013	0.014	13	13	13	12
C11	23	04 40 59.4	+44 30 07	1.6	14.444	13.717	13.288	12.774	0.010	0.009	0.013	0.017	15	15	15	14
1A 0535+262																
C1	2	05 39 09.6	+26 22 48	5.0	11.047	10.754	10.578	10.327	0.013	0.009	0.014	0.019	7	7	7	6
C2	4	05 39 09.5	+26 22 25	4.7	10.211	10.081	9.994	9.878	0.014	0.010	0.014	0.018	7	7	7	6
C3	7	05 38 56.9	+26 21 27	2.5	14.029	13.240	12.788	12.327	0.012	0.012	0.014	0.011	7	7	7	6
C4	15	05 39 01.9	+26 20 34	2.2	14.735	13.802	13.256	12.656	0.012	0.009	0.016	0.022	7	7	7	6
C5	17	05 38 47.6	+26 20 17	2.0	13.231	12.705	12.389	12.001	0.010	0.009	0.011	0.014	7	7	7	6
C6	26	05 39 09.2	+26 18 42	3.2	14.080	13.355	12.940	12.528	0.014	0.011	0.013	0.019	7	7	7	6
C7	33	05 38 41.6	+26 17 17	3.2	14.761	13.981	13.544	13.101	0.016	0.012	0.016	0.023	7	7	7	6
IGR J06074+2205																
C1	18	06 07 12.0	+22 07 42	3.9	15.033	14.450	14.145	13.733	0.019	0.011	0.017	0.019	6	6	6	6
C2	22	06 07 14.8	+22 07 18	3.0	14.711	14.011	13.615	13.192	0.021	0.017	0.016	0.026	6	6	6	6
C3	25	06 07 32.2	+22 07 04	1.8	14.522	13.717	13.275	12.859	0.017	0.014	0.013	0.022	6	6	6	6
C4	51	06 07 22.8	+22 05 03	1.1	14.856	14.203	13.817	13.417	0.021	0.015	0.015	0.028	6	6	6	6
C5	64	06 07 15.3	+22 03 35	3.4	14.695	14.077	13.750	13.325	0.023	0.016	0.018	0.020	6	6	6	6
C6	66	06 07 26.3	+22 03 06	2.6	14.611	13.914	13.513	13.102	0.013	0.015	0.014	0.018	6	6	6	6
C7	75	06 07 20.6	+22 01 53	4.2	14.625	14.151	13.878	13.526	0.021	0.007	0.014	0.024	6	6	6	6
C8	79	06 07 36.6	+22 01 15	5.0	15.185	14.411	13.970	13.512	0.020	0.020	0.013	0.025	6	6	6	6
4U J1845.0-0433																
C1	13	18 45 04.5	-04 30 32	3.4	16.153	15.082	14.439	13.768	0.012	0.010	0.007	0.011	10	10	10	9
C2	19	18 45 02.9	-04 31 27	2.5	15.394	14.298	13.661	12.940	0.014	0.013	0.007	0.005	11	11	10	9
C3	27	18 45 06.6	-04 31 50	2.4	16.476	14.651	13.518	12.402	0.014	0.009	0.009	0.009	11	11	11	9
C4	33	18 44 49.0	-04 32 19	3.5	16.183	15.008	14.300	13.498	0.013	0.008	0.007	0.007	11	11	11	9
C5	39	18 44 49.5	-04 32 45	3.1	15.107	13.958	13.266	12.472	0.013	0.008	0.007	0.006	11	11	11	9
C6	42	18 45 01.1	-04 33 07	0.8	15.647	14.620	14.013	13.336	0.011	0.010	0.007	0.011	11	11	11	10
C7	47	18 45 10.3	-04 33 38	2.1	15.226	14.151	13.496	12.803	0.011	0.010	0.007	0.011	11	11	11	10
C8	55	18 45 08.3	-04 34 13	1.6	16.651	15.126	14.115	13.058	0.012	0.008	0.008	0.008	11	11	11	9
C9	56	18 45 16.1	-04 34 19	3.6	15.914	14.841	14.188	13.508	0.012	0.008	0.008	0.011	10	10	10	10
C10	59	18 45 12.1	-04 34 22	2.6	16.707	14.813	13.728	12.698	0.013	0.009	0.009	0.009	11	11	11	9
C11	79	18 44 48.7	-04 36 23	3.9	16.292	15.168	14.487	13.753	0.014	0.009	0.008	0.018	10	10	10	10
C12	89	18 44 56.8	-04 37 06	3.2	17.287	15.162	13.827	12.559	0.014	0.008	0.009	0.009	10	10	11	9

**Table A.4.** Secondary standards in the field of view of high-mass X-ray binaries (cont.)

Star	ID	RA	DEC	d (')	$\bar{B}$ (mag)	$\bar{V}$ (mag)	$\bar{R}$ (mag)	$\bar{I}$ (mag)	$\sigma_{\bar{B}}$ (mag)	$\sigma_{\bar{V}}$ (mag)	$\sigma_{\bar{R}}$ (mag)	$\sigma_{\bar{I}}$ (mag)	$N_B$	$N_V$	$N_R$	$N_I$
4U 1907+09																
C1	41	19 09 43.2	+09 51 59	2.5	18.522	16.935	15.971	15.100	0.008	0.005	0.008	0.007	11	11	12	8
C2	42	19 09 40.2	+09 51 51	2.1	18.873	17.103	16.050	14.920	0.012	0.010	0.013	0.015	12	11	12	8
C3	47	19 09 27.4	+09 51 06	2.8	17.018	15.383	14.461	13.533	0.009	0.005	0.007	0.007	13	13	13	10
C4	52	19 09 26.7	+09 50 53	2.9	17.795	16.203	15.274	14.257	0.013	0.011	0.008	0.013	12	13	13	10
C5	55	19 09 31.7	+09 50 15	1.6	18.191	16.759	15.908	15.014	0.010	0.011	0.009	0.010	12	13	13	10
C6	70	19 09 37.6	+09 49 54	0.1	17.608	16.034	15.137	14.208	0.011	0.006	0.008	0.007	13	13	14	10
C7	77	19 09 38.0	+09 49 47	1.6	17.214	15.281	14.166	13.095	0.009	0.010	0.007	0.010	12	13	13	10
C8	119	19 09 23.0	+09 47 25	4.3	18.419	16.995	16.126	15.314	0.013	0.007	0.010	0.012	9	9	9	7
C9	142	19 09 28.7	+09 47 03	3.5	18.104	16.545	15.501	14.560	0.015	0.004	0.011	0.009	10	10	10	8
C10	146	19 09 37.0	+09 46 40	3.1	17.196	15.541	14.559	13.477	0.010	0.004	0.008	0.007	11	11	11	8
XTE J1946+274																
C1	55	19 45 44.7	+27 24 27	2.7	14.969	14.109	13.607	13.117	0.010	0.006	0.006	0.009	7	7	7	7
C2	62	19 45 54.2	+27 24 13	4.0	15.723	14.309	13.506	12.746	0.011	0.006	0.007	0.009	7	7	7	7
C3	92	19 45 56.8	+27 22 50	3.9	17.499	15.666	14.590	13.587	0.011	0.014	0.008	0.011	7	7	7	7
C4	97	19 45 58.3	+27 22 38	4.2	16.411	15.443	14.862	14.294	0.008	0.005	0.010	0.007	7	7	7	7
C5	108	19 45 44.4	+27 22 18	1.1	16.554	15.053	14.217	13.456	0.010	0.007	0.009	0.013	7	7	7	7
C6	137	19 45 27.7	+27 20 52	2.7	16.304	15.443	14.911	14.363	0.009	0.007	0.010	0.006	7	7	7	7
C7	140	19 45 38.5	+27 20 47	1.1	17.156	15.530	14.607	13.732	0.015	0.011	0.013	0.015	7	7	7	7
C8	161	19 45 43.0	+27 19 44	2.3	15.235	14.354	13.822	13.291	0.008	0.005	0.007	0.010	7	7	7	7
C9	164	19 45 37.4	+27 19 40	2.3	17.185	15.144	13.948	12.823	0.012	0.010	0.011	0.023	7	7	7	7
C10	166	19 45 45.3	+27 19 38	2.6	16.886	15.243	14.275	13.371	0.018	0.008	0.009	0.011	7	7	7	7
C11	167	19 45 46.9	+27 19 35	2.8	16.984	15.881	15.271	14.670	0.012	0.012	0.008	0.015	7	7	7	7
KS 1947+300																
C1	99	19 49 41.5	+30 13 47	1.8	15.329	14.504	14.002	13.537	0.006	0.006	0.006	0.009	17	17	17	14
C2	103	19 49 18.4	+30 13 42	3.8	15.129	13.709	12.900	12.184	0.004	0.004	0.004	0.006	16	17	15	14
C3	124	19 49 19.3	+30 12 49	3.4	13.409	12.856	12.524	12.236	0.009	0.008	0.008	0.015	10	10	9	9
C4	133	19 49 31.4	+30 12 35	0.8	13.625	13.097	12.772	12.459	0.007	0.008	0.006	0.017	14	14	12	11
C5	150	19 49 55.1	+30 12 16	4.2	14.200	13.742	13.451	13.140	0.012	0.009	0.004	0.012	9	9	9	9
C6	191	19 49 38.3	+30 10 56	1.7	14.545	13.840	13.414	13.041	0.006	0.006	0.004	0.011	17	18	17	15
C7	192	19 49 40.0	+30 10 55	1.8	15.179	14.155	13.501	12.983	0.005	0.006	0.006	0.011	16	18	18	15
C8	208	19 49 14.3	+30 10 27	5.0	14.154	13.484	13.074	12.708	0.007	0.007	0.005	0.011	13	13	13	11
C9	224	19 49 39.1	+30 09 26	3.1	14.694	13.960	13.496	13.079	0.008	0.007	0.006	0.012	17	17	17	15
C10	228	19 49 46.2	+30 09 17	3.9	15.014	14.313	13.873	13.477	0.006	0.006	0.004	0.009	16	18	18	14
EXO 2030+375																
C1	56	20 32 10.1	+37 39 56	1.9	16.567	15.586	15.034	14.512	0.009	0.007	0.009	0.009	9	9	9	9
C2	63	20 32 22.8	+37 39 00	1.6	18.414	16.949	16.066	15.248	0.016	0.008	0.012	0.025	9	9	9	9
C3	72	20 32 27.5	+37 38 13	2.4	17.735	16.462	15.683	14.879	0.021	0.013	0.008	0.011	7	7	7	7
C4	77	20 32 34.2	+37 37 17	3.3	17.941	16.634	15.882	15.189	0.012	0.011	0.009	0.011	9	9	9	9
C5	80	20 32 26.5	+37 37 07	2.5	18.321	17.058	16.328	15.662	0.012	0.010	0.009	0.010	9	9	9	9
C6	81	20 32 21.5	+37 37 01	1.7	18.622	16.746	15.440	14.074	0.010	0.011	0.010	0.013	9	9	9	9
C7	83	20 32 07.7	+37 36 56	1.9	18.414	17.044	16.237	15.424	0.012	0.011	0.009	0.009	9	9	9	9
C8	88	20 32 16.4	+37 36 21	1.9	17.778	16.636	15.943	15.355	0.010	0.011	0.008	0.026	9	9	9	9
C9	101	20 31 55.3	+37 36 14	4.3	17.403	16.102	15.359	14.628	0.012	0.011	0.010	0.010	8	8	8	8
C10	148	20 32 14.7	+37 35 46	2.5	17.331	16.108	15.405	14.712	0.017	0.014	0.013	0.013	9	9	9	9
C11	160	20 32 18.8	+37 34 56	3.4	17.019	15.467	14.487	13.454	0.014	0.013	0.011	0.016	9	9	8	8
C12	183	20 32 14.2	+37 34 14	4.1	17.793	16.510	15.704	15.068	0.014	0.010	0.009	0.015	9	9	9	9

**Table A.5.** Secondary standards in the field of view of high-mass X-ray binaries (cont.)

Star	ID	RA	DEC	d (')	$\bar{B}$ (mag)	$\bar{V}$ (mag)	$\bar{R}$ (mag)	$\bar{I}$ (mag)	$\sigma_{\bar{B}}$ (mag)	$\sigma_{\bar{V}}$ (mag)	$\sigma_{\bar{R}}$ (mag)	$\sigma_{\bar{I}}$ (mag)	$N_B$	$N_V$	$N_R$	$N_I$
GRO J2058+42																
C1	19	20 59 00.7	+41 50 06	4.3	15.217	14.318	13.786	13.157	0.006	0.006	0.005	0.009	14	14	14	12
C2	33	20 58 59.5	+41 49 02	3.3	14.392	13.575	13.101	12.600	0.011	0.005	0.005	0.009	14	14	14	12
C3	45	20 58 30.5	+41 48 14	3.5	15.672	14.301	13.482	12.583	0.010	0.004	0.004	0.007	17	17	17	15
C4	50	20 58 38.0	+41 47 52	2.0	15.590	14.482	13.832	13.161	0.010	0.004	0.006	0.011	19	19	19	16
C5	83	20 59 08.8	+41 46 24	3.9	15.743	14.877	14.377	13.922	0.011	0.007	0.006	0.007	15	15	15	13
C6	90	20 58 46.0	+41 45 57	0.7	15.494	14.622	14.092	13.550	0.009	0.006	0.006	0.005	21	21	21	18
C7	91	20 58 44.5	+41 45 51	0.9	14.990	14.057	13.511	12.936	0.008	0.005	0.004	0.005	21	21	21	18
C8	100	20 59 05.5	+41 44 20	4.0	15.422	14.339	13.711	13.011	0.009	0.006	0.005	0.007	18	18	18	16
C9	101	20 59 09.0	+41 44 05	4.7	16.455	15.136	14.352	13.528	0.013	0.006	0.006	0.011	15	15	15	14
SAX J2103.5+4545																
C1	27	21 03 35.7	+45 47 57	2.8	15.784	14.772	14.145	13.538	0.010	0.006	0.003	0.012	10	9	10	9
C2	61	21 03 51.2	+45 47 20	3.4	15.381	14.664	14.221	13.759	0.013	0.006	0.006	0.009	11	10	11	10
C3	69	21 03 10.2	+45 47 04	4.8	16.016	14.875	14.138	13.391	0.011	0.007	0.007	0.011	10	9	10	9
C4	72	21 03 36.0	+45 46 37	1.4	15.660	14.465	13.710	12.969	0.007	0.005	0.005	0.008	17	16	17	14
C5	100	21 03 36.4	+45 45 23	0.3	14.861	14.080	13.609	13.153	0.006	0.006	0.006	0.010	18	18	19	16
C6	104	21 03 20.2	+45 45 15	2.7	15.108	13.585	12.672	11.810	0.008	0.004	0.006	0.007	19	18	12	16
C7	113	21 03 17.2	+45 44 56	3.2	16.022	14.772	13.982	13.200	0.006	0.004	0.004	0.007	18	18	19	16
C8	114	21 03 22.0	+45 44 56	2.4	15.776	14.690	14.024	13.399	0.006	0.005	0.005	0.006	18	18	19	16
C9	120	21 03 27.8	+45 44 36	1.4	15.162	14.302	13.752	13.192	0.009	0.006	0.006	0.010	19	18	19	16
C10	131	21 03 29.5	+45 43 58	1.5	15.124	14.190	13.606	13.020	0.007	0.005	0.004	0.005	18	18	19	16
C11	136	21 03 10.0	+45 43 34	4.6	15.265	14.348	13.768	13.156	0.008	0.006	0.006	0.009	14	13	14	12
C12	138	21 03 30.3	+45 43 29	1.8	15.512	14.697	14.183	13.638	0.007	0.005	0.004	0.007	18	18	19	16
C13	150	21 03 42.2	+45 42 30	2.7	14.680	14.166	13.848	13.471	0.007	0.005	0.006	0.007	18	18	19	16
C14	170	21 03 52.4	+45 40 49	5.1	15.248	14.424	13.937	13.479	0.007	0.005	0.006	0.009	14	14	15	14
IGR J21343+4738																
C1	7	21 33 55.5	+47 42 37	6.2	15.332	14.446	13.889	13.309	0.006	0.016	0.012	0.011	5	5	5	5
C2	15	21 33 55.7	+47 42 00	5.7	14.375	13.607	13.104	12.562	0.006	0.014	0.011	0.012	5	5	5	5
C3	25	21 34 09.0	+47 41 07	3.6	14.357	13.632	13.203	12.744	0.010	0.011	0.012	0.010	6	6	5	6
C4	41	21 33 57.5	+47 40 16	4.4	14.796	13.958	13.450	12.935	0.007	0.011	0.009	0.009	6	6	6	6
C5	60	21 34 30.9	+47 39 34	2.3	15.206	14.356	13.842	13.349	0.008	0.011	0.009	0.010	6	6	6	6
C6	73	21 34 38.7	+47 38 19	3.0	14.350	13.683	13.265	12.840	0.008	0.013	0.012	0.012	6	6	5	6
C7	78	21 34 30.3	+47 38 03	1.6	15.293	14.432	13.917	13.439	0.009	0.012	0.011	0.010	6	6	6	6
C8	80	21 34 35.0	+47 37 55	2.4	14.391	14.014	13.785	13.513	0.010	0.014	0.011	0.014	6	6	6	6
C9	95	21 34 45.3	+47 37 30	4.1	14.916	14.018	14.106	13.783	0.008	0.015	0.013	0.017	5	5	5	5
C10	103	21 34 12.3	+47 37 28	1.3	15.133	14.157	13.584	13.092	0.008	0.013	0.010	0.010	6	6	6	6
C11	112	21 34 24.7	+47 36 46	1.4	14.636	13.865	13.395	12.924	0.009	0.012	0.010	0.012	6	6	6	6
C12	116	21 34 44.3	+47 36 17	4.4	14.879	14.113	13.634	13.173	0.007	0.014	0.012	0.015	5	5	5	5
C13	148	21 33 59.1	+47 34 22	5.0	14.529	13.763	13.307	12.859	0.009	0.012	0.010	0.011	6	6	6	6

**Table A.6.** Secondary standards in the field of view of high-mass X-ray binaries (cont.)

Star	ID	RA	DEC	d ( $^{\circ}$ )	$\bar{B}$ (mag)	$\bar{V}$ (mag)	$\bar{R}$ (mag)	$\bar{I}$ (mag)	$\sigma_{\bar{B}}$ (mag)	$\sigma_{\bar{V}}$ (mag)	$\sigma_{\bar{R}}$ (mag)	$\sigma_{\bar{I}}$ (mag)	$N_B$	$N_V$	$N_R$	$N_I$
4U 2206+54																
C1	20	22 07 59.0	+54 33 53	2.8	13.349	12.902	12.651	12.371	0.006	0.004	0.002	0.007	25	22	23	21
C2	37	22 08 20.1	+54 32 53	3.9	14.405	13.766	13.381	12.934	0.007	0.004	0.005	0.005	26	23	24	22
C3	41	22 07 30.2	+54 32 47	4.0	14.009	13.633	13.400	13.104	0.007	0.007	0.008	0.008	16	16	16	15
C4	69	22 08 05.0	+54 30 52	1.3	14.496	13.753	13.297	12.868	0.009	0.005	0.003	0.005	28	24	25	23
C5	77	22 08 20.8	+54 30 33	3.5	10.648	10.429	10.284	10.120	0.017	0.006	0.005	0.006	27	27	27	24
C6	84	22 07 48.2	+54 30 17	1.4	13.784	13.132	12.732	12.353	0.006	0.005	0.003	0.005	28	25	24	24
C7	97	22 08 25.4	+54 29 07	4.6	12.161	11.950	11.789	11.628	0.007	0.005	0.004	0.007	22	19	20	20
C8	99	22 08 15.4	+54 28 56	3.4	14.320	13.806	13.489	13.163	0.006	0.004	0.004	0.006	28	24	26	25
C9	111	22 07 59.4	+54 28 05	2.9	13.875	13.266	12.880	12.508	0.007	0.004	0.004	0.005	28	26	26	24
C10	117	22 08 01.0	+54 27 42	3.4	12.376	11.835	11.504	11.171	0.006	0.004	0.003	0.006	27	25	27	24
SAX J2239.3+6116																
C1	21	22 39 16.7	+61 18 19	1.9	17.859	16.425	15.561	14.718	0.009	0.013	0.011	0.007	7	7	7	7
C2	25	22 39 12.5	+61 17 12	1.2	15.848	14.774	14.158	13.515	0.011	0.012	0.011	0.009	7	7	7	7
C3	27	22 39 14.8	+61 17 08	1.0	18.178	16.433	15.362	14.247	0.008	0.012	0.010	0.008	7	7	7	7
C4	28	22 39 32.9	+61 17 04	1.5	18.119	16.778	16.013	15.120	0.010	0.014	0.009	0.008	7	7	7	7
C5	29	22 39 34.7	+61 16 44	1.7	17.666	16.351	15.580	14.717	0.008	0.013	0.013	0.013	7	7	7	7
C6	31	22 38 54.6	+61 16 36	3.1	16.242	15.142	14.484	13.804	0.010	0.012	0.009	0.008	7	7	7	7
C7	39	22 38 53.0	+61 16 04	3.3	17.610	16.252	15.373	14.629	0.012	0.014	0.010	0.008	7	7	7	7
C8	40	22 39 38.2	+61 15 50	2.2	16.394	15.249	14.560	13.867	0.013	0.012	0.010	0.007	7	7	7	7
C9	41	22 39 30.3	+61 15 45	1.3	16.748	15.656	15.022	14.321	0.011	0.010	0.009	0.008	7	7	7	7
C10	45	22 39 35.7	+61 15 10	2.1	16.076	14.974	14.336	13.748	0.010	0.010	0.010	0.007	7	7	7	7
C11	47	22 39 48.9	+61 15 03	3.6	18.107	16.495	15.516	14.531	0.009	0.013	0.013	0.007	7	7	7	7
C12	50	22 39 43.5	+61 14 38	3.2	17.323	16.028	15.249	14.483	0.011	0.014	0.011	0.010	7	7	7	7



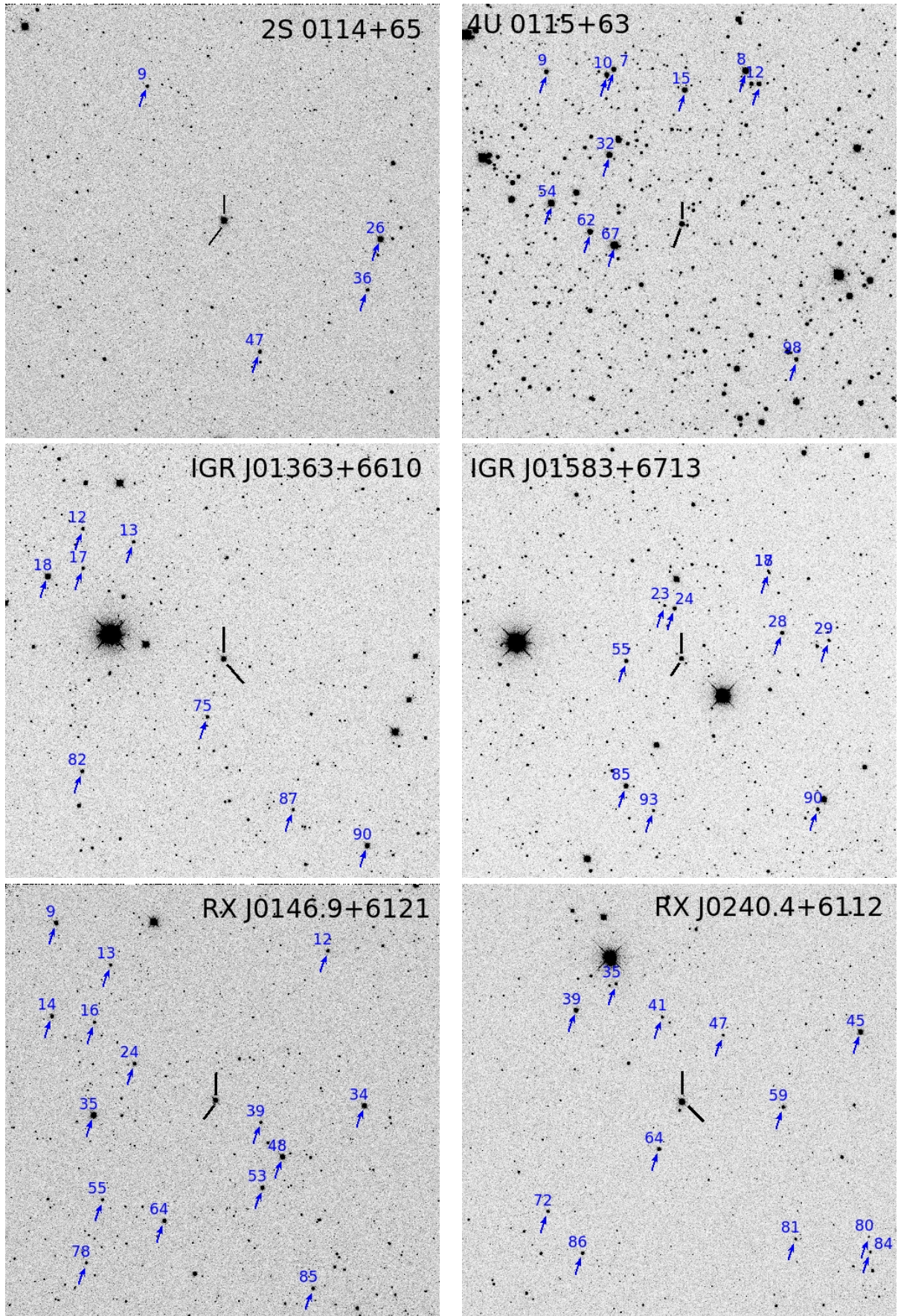


**Fig. A.1.** Bias-subtracted and flat field-corrected R-band images obtained with the 1.3 m telescope of the Skinakas observatory. Arrows mark the position of the secondary standards. North is up, east is left. The field of view is  $\sim 9.5' \times 9.5'$ . The target lies in the centre of the image and it is marked with two lines.



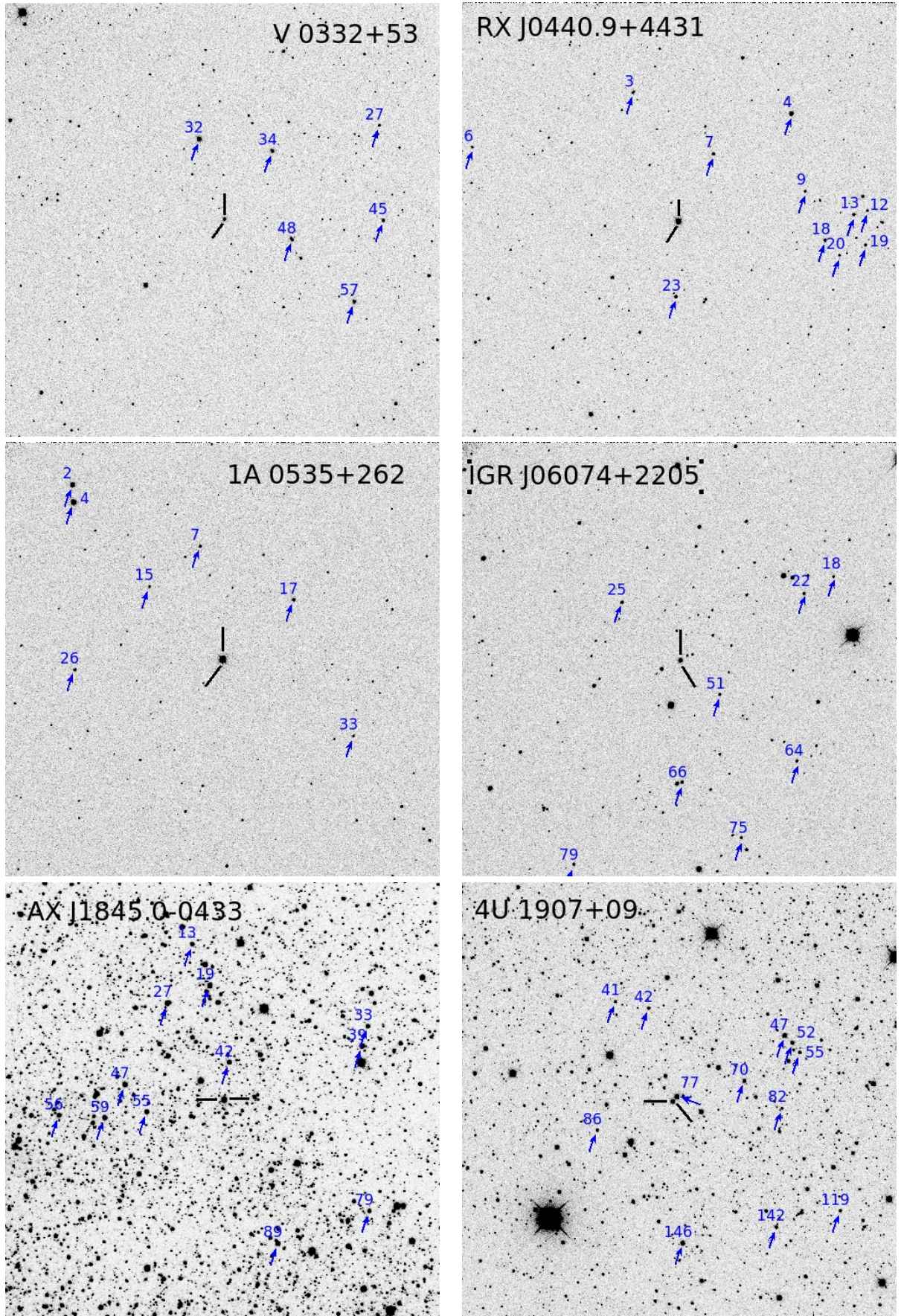


**Fig. A.2.** Bias-subtracted and flat field-corrected R-band images obtained with the 1.3 m telescope of the Skinakas observatory. Arrows mark the position of the secondary standards. North is up, east is left. The field of view is  $\sim 9.5' \times 9.5'$ . The target lies in the centre of the image and it is marked with two lines.



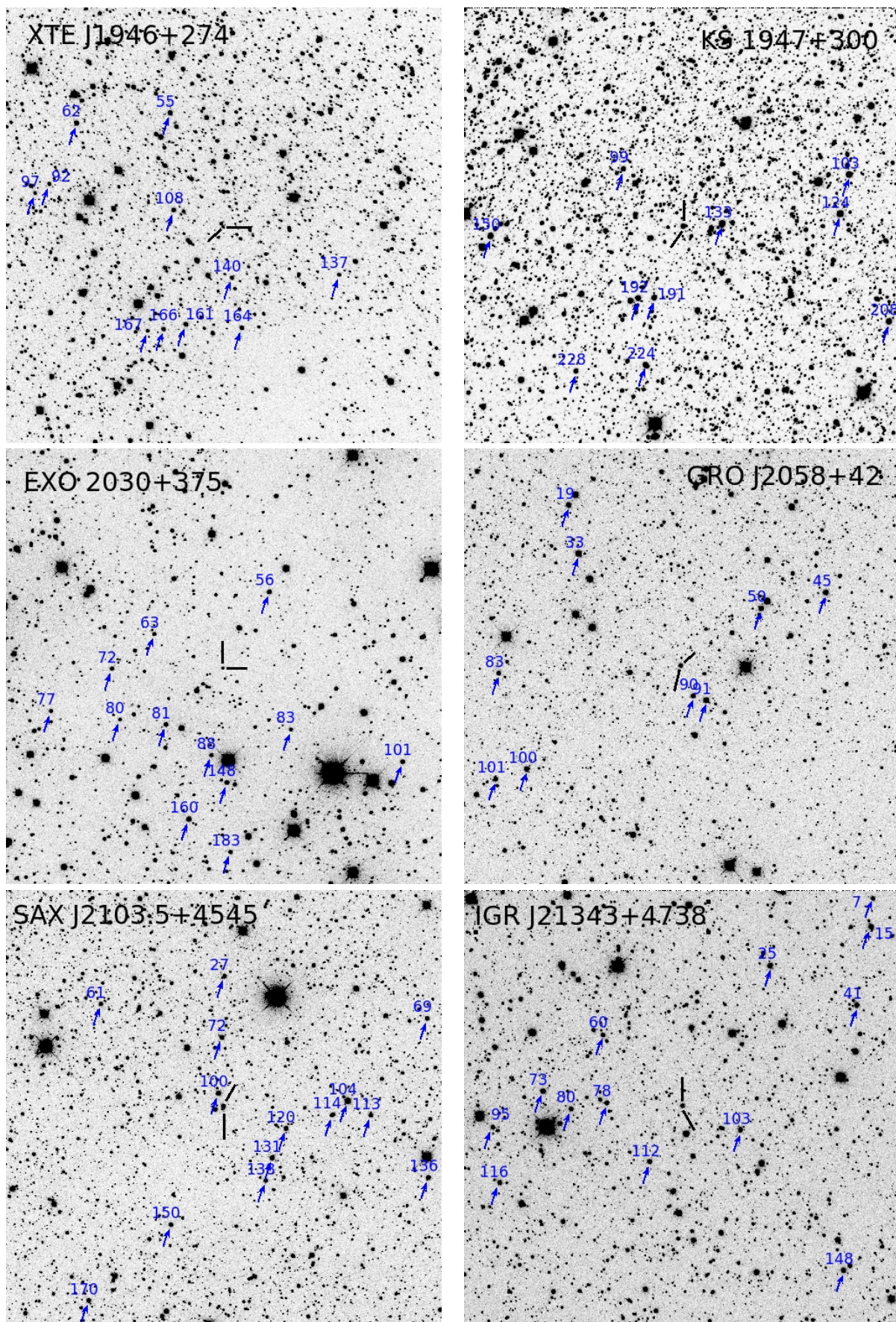


**Fig. A.3.** Bias-subtracted and flat field-corrected R-band images obtained with the 1.3 m telescope of the Skinakas observatory. Arrows mark the position of the secondary standards. North is up, east is left. The field of view is  $\sim 9.5' \times 9.5'$ . The target lies in the centre of the image and it is marked with two lines.



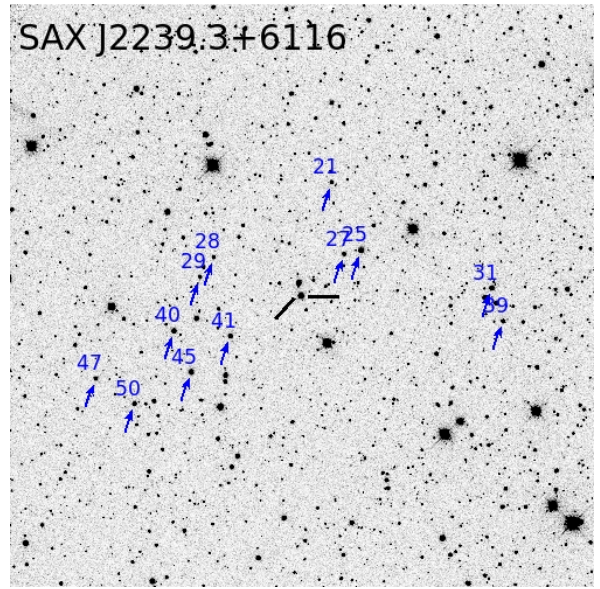
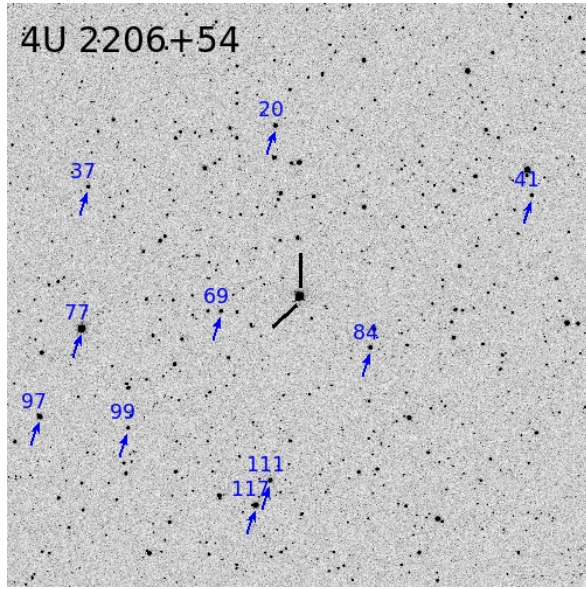


**Fig. A.4.** Bias-subtracted and flat field-corrected R-band images obtained with the 1.3 m telescope of the Skinakas observatory. Arrows mark the position of the secondary standards. North is up, east is left. The field of view is  $\sim 9.5' \times 9.5'$ . The target lies in the centre of the image and it is marked with two lines.